The International Young Researchers' Conference
DOI: doi.org/10.34614/iyrc0056

Fabrication of a microfluidic tumor-on-a-chip model for personalized cancer therapy

Shailesh Senthil Kumar
Lynbrook High School, United States
skshailesh@gmail.com

Abstract

Cancer has had a defining impact on medicine for the past few decades, and its effects can be felt worldwide, with 91 out of 172 countries listing it as their first or second cause of mortality before the age of 70. However, cancer has shown a significantly low turnout for clinical use of anti-cancer drugs, with less than 10 percent of these drugs entering the market. Current models are not sufficient and fail to reproduce the human body's environment in two key ways. First, three-dimensional human tumors' biophysical and biochemical aspects drastically change tumor susceptibility due to shear stress and extracellular matrix production. Cancer drug screening has a second hurdle: each person's tumor is different, caused by DNA mutations, RNA regulation, and the proteins expressed. Cancer cells have demonstrated intratumoral heterogeneity within tumors, allowing cell subtypes to be artificially selected against therapeutics. Therefore, tumors require a personalized and precise form of medicine suited for the new age of personalized patient therapy. A microfluidic 3D model is required to replicate a three-dimensional tumor microenvironment, incorporating model blood vessels and embedded tumor spheroids to allow 3D tumoroids to form. The project hopes to pair this highly replicable and reusable microfluidic device with microscopy to characterize phenotypic heterogeneity spatially and temporally. Specific factors cell cycle patterns, necrosis, cell size, and motility will be analyzed to evaluate tumor aggressiveness and identify tumor subtypes for personalized therapy.

Keywords: tumor heterogeneity, microfluidics, oncology

Introduction

Cancer has had a defining impact on medicine for the past few decades, with more than 20 countries listing cancer as their third or fourth highest cause of death, and 91 out of 172 countries listing it as their first or second cause of mortality before the age of 70. These patient numbers continue to grow, creating increased pressure for drug screening (Bray, 2018). However, cancer has also demonstrated significantly low turnout for anti-cancer drugs' clinical use, with less than 10 percent of these drugs entering the market from preclinical trials (Hutchinson, 2011). One of the leading causes of the phenomenon is the models used to test these drugs during trials. Current models, including in vitro and animal models, are ineffective and fail to reproduce the tumor's relationship with the human body in two ways.

First, the gold-standard of in vitro trials, two-dimensional models like petri dishes, do not reproduce the three-dimensional nature of human

tumors. The three-dimensional tumor microenvironment incorporates biophysical factors like shear stress and structural components such as the extracellular matrix. These differences cause drastic changes in the cells being studied and affect tumor drug susceptibility, which changes cancer's response to therapeutics (Mierke, 2019). The most popular three-dimensional model, animal or xenograft models, are accompanied by ethical concerns, and variables are not effectively regulated (Begley, 2012). Other popular three-dimensional models rely on scaffolds that assist in the cell's three-dimensional formation. Therefore, alternative methods of modeling the tumor microenvironment are necessary.

Cancer drug screening has a second hurdle: each patient's tumor is unique. Within tumors, cancer cells have demonstrated the phenomenon of intratumoral heterogeneity, displaying a variety of cancer subtypes, which exacerbates the failure of anti-cancer therapeutics (Oudin 2016). Cells in two-dimensional models lose heterogeneity in their phenotype, excluding aggressive cancer subtypes from therapeutic trials. In a natural environment, therapeutics select for aggressive subtypes, similar to the bacterial response to antibiotics (Chapman, 2014). Therapeutic-resistant subtypes prevail within a tumor and the cancer metastasizes. Therefore, tumors require a personalized and precise form of medicine that targets multiple subtypes and is more prevalent in the new age of personalized patient therapy.

This study addresses the drawbacks of current cancer models. The three-dimensional environment's biochemical and biophysical factors are reproduced through microfluidics to support intratumoral heterogeneity. Setbacks in animal models are addressed by recapitulating conditions in the body like shear stress, nutrient transfer, and waste removal in a highly replicable and reusable microfluidic model. By pairing this device with microscopy and computer vision, the project hopes to identify phenotypic heterogeneity spatially. Cell cycle patterns, necrosis, cell size, and motility will be analyzed to evaluate tumor aggressiveness and identify tumor subtypes.

Experimental Methods

General Methods

A polydimethylsiloxane (PDMS) microfluidic device from a 3D-printed mold produced the tumoroids. A549 lung epithelial cells were cultured in a monolayer and split biweekly for three months to promote a culture with increased heterogeneity. After multiple experiments with A549 cells, the device structure was optimized to identify a model that could promote freely forming three-dimensional structures. Once the device was created, the hypothesized heterogeneous factors were identified and quantified using fluorescence microscopy and a cell counter (Figure 1).

Device Fabrication

The device's channels and cell growth chamber were molded using a 3D-printed mold designed in AutoDesk Fusion. The general mold features the main channel, space for an agarose barrier, and chambers for cancer cells to be deposited and form tumoroids. Prototypes were tested based on imaging quality, the visibility of the tumoroids, and its promotion of three-dimensional tumoroids.

The material used, polydimethylsiloxane (PDMS), is commonly grouped as a silicon-based organic polymer. Twenty-eight grams of the elastomer base is mixed with 4 grams of the elastomer curing agent with a ratio of 1:7 for 10 minutes to create the PDMS elastomer. The elastomer mixture is then desiccated for five minutes to remove bubbles from the liquid mixture. After this process, the mixture is poured into the center of a sterilized petri dish with the mold. Twenty-four hours later, the elastomer mixture should completely solidify and cut out of the petri dish. The 1% agarose barrier is then added into the PDMS cast which is placed between two 6 cm^2 sheets of plexiglass. One of these plexiglass

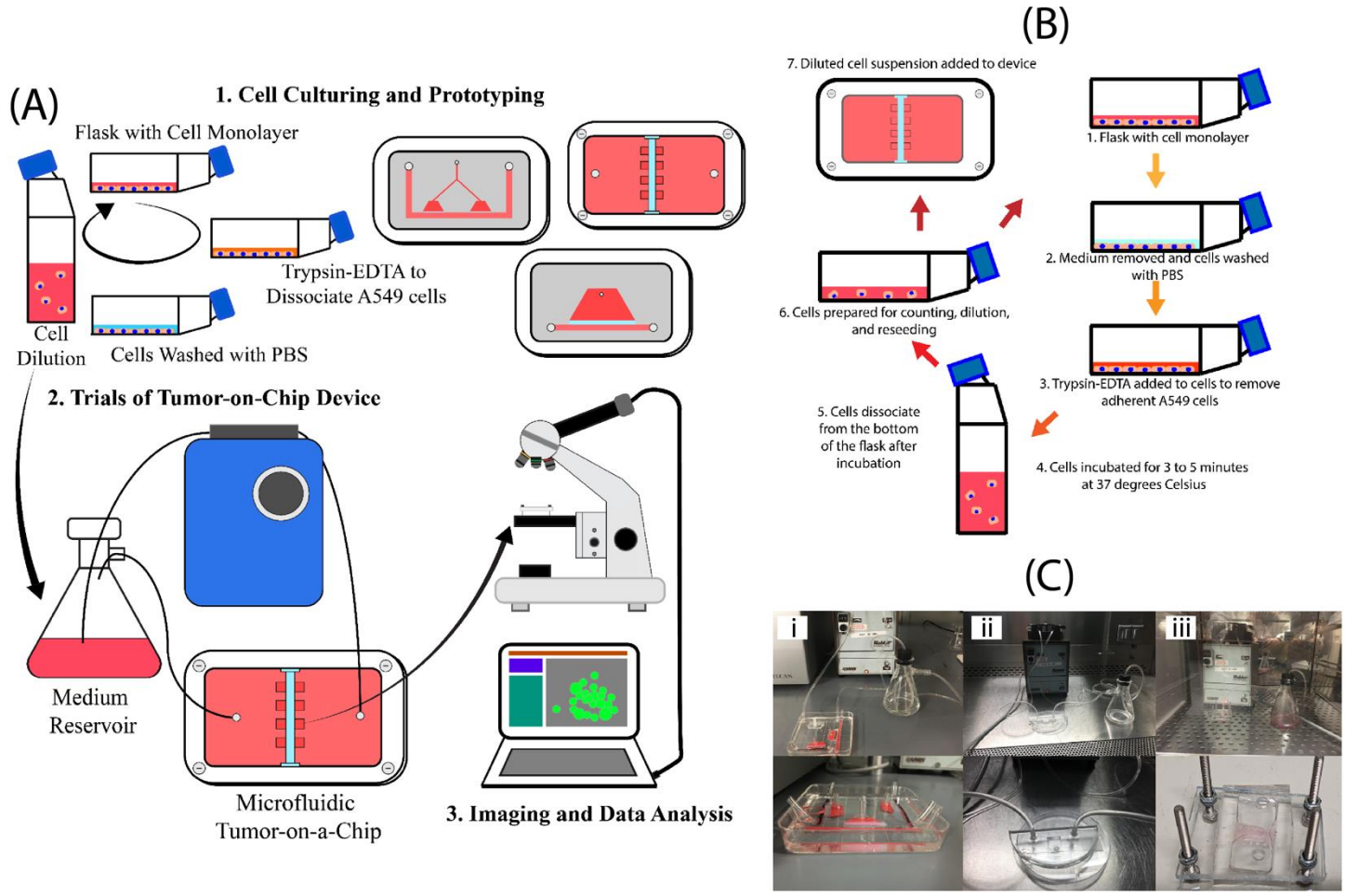

FIGURE 1. (A) Overall diagram of full procedure from cell culturing and prototype design to analysis of cells in device. (B) Diagram of cell splitting procedure used to promote heterogeneity and seed cells in tumor-on-a-chip device. (C) Different prototype models in device setup (i) First prototype design with scotch tape mold and petri dish base (ii) second prototype using glass slide (iii) Final prototype design with medium flow above cancer growth chamber and plexiglass cover and base.

sheets was drilled to incorporate inlets and outlets for the peristaltic pump tubing, and this three-part structure was sealed together using screws.

Cell Culture

A549 lung epithelial cells were used in this experiment due to their resilience. These cells do not regularly display heterogeneity within the cell line as they are conditioned to be grown in a monolayer. Therefore, to promote mutations in the cells, the A549 cells were cultured in F-12 medium with added Fetal Gro and split biweekly for three months. At this high passage count, the cells develop mutations and can be tested in microfluidic models.

The cells were grown in T75 cell culture flasks at a splitting ratio of 1:5 to maintain the culture. The cell splitting or subculture protocol, specific to adherent cell lines, is as follows: PBS, trypsin-EDTA, and F-12 medium with Fetal Gro are warmed to room temperature 37˚C water broth. The flask containing the A549 cells is aspirated using a suction line. 15 mL of 1xPBS (0.2 mL of PBS/cm2) is added to the flask and aspirated out after one minute. Then, 3 mL of trypsin-EDTA is added, and the cells are incubated for three to five minutes at 37˚C in an incubator. 7 mL of F-12 medium with FetalGro is then added to the flask, and the cells are dispersed using a serological pipette. 2 mL of this

mixture is added to a new flask with 15 mL of F-12 medium with FetalGro.

Cell Seeding

The A549 adherent cell lines were trypsinized and diluted to 0.5 x 10^6 cells/mL to seed the cells within the device. To trypsinize the cells, 3 mL of trypsin-EDTA is added to the cell culture, and the flask is incubated at 37˚C for three to five minutes. After the cells are dispersed using a serological pipette, the cell count is quantified using a cell counter (This specific procedure is for the DeNovix CellDrop). Ten microliters of the A549 cells are removed from the flask using a micropipette and added to 10 microliters of alamarBlue. This mixture is then pipetted into the cell drop, and the cell concentration is quantified. F-12 broth is added to reduce the concentration to 0.5 x 10^6 cells per milliliter. Then, 0.833 mL of this dilution is then added to 5mL of the medium and this dilution is run through the peristaltic pump at 2.5 microliter/min after the pump's tubing is inserted into the inlet and outlet of the prototype.

Prototype Device

After seeding the cells, F-12 medium passes through the tubing at 2.5 microliter/min throughout the experiment. Every four hours, the tumoroids are imaged to identify three-dimensional structures to quantify the prototype's effectiveness.

Identifying Intratumoral Heterogeneity

The procedure for running the device is the same as the prototyping methods with the addition of a cell cycle marker (FUCCI Cell Cycle Sensor) to track the tumor areas that were dormant or were actively growing. One-hundred microliters of the cell cycle marker were added to the microfluidic device overnight to stain the cells. Phenotypic differences in cell size and cell motility were quantified based on microscope images taken every four hours. Cell size data was also verified using a cell counter at the end of each experiment and movement was analyzed over time using these images. Cell cycle patterns were identified using the cell cycle marker based on green or red fluorescence. Then, spatial patterns were identified by grouping consistent cell characteristics. This data was used as a sample dataset to create a computer vision model that used parts of the object-detection "YOLO" algorithm to identify cells in the microscope images (Redmon, 2015). The specific algorithm was selected as it ran efficiently and could be easily integrated into the data analysis pipeline. This model can be used to identify heterogeneity in the device from light and fluorescence microscope images for future studies.

Results

Prototyping the Device

The final prototype of the tumor-on-a-chip could produce an average of eight tumoroids per trial. In this study, a tumoroid is characterized as a mass of cancer cells with a three-dimensional structure, more than 30 cells, and active cell motility. These cells were differentiated from the monolayer because A549 cells have a distinct rhombus shape when attached as a monolayer. The final prototype was created using PDMS from a 3D-printed mold, and the cells were grown on plexiglass for imaging purposes. This final prototype was a culmination of 25 trials with three distinct prototypes (Figure 2).

The first design was molded using scotch tape to achieve a height in nanometers and centered on the horizontal axis. It featured two arms for the inlet and outlet and the main channel separated by a 1% agarose barrier from two cell growth chambers that branched upwards towards a cell seeding inlet. The tape created rough molds that caused medium leakage after the PDMS and base were sealed together and made it difficult to image the cells under a microscope. The prototype averaged zero tumoroids for five trials and was discarded. However, the cells formed a monolayer within the two cell growth chambers.

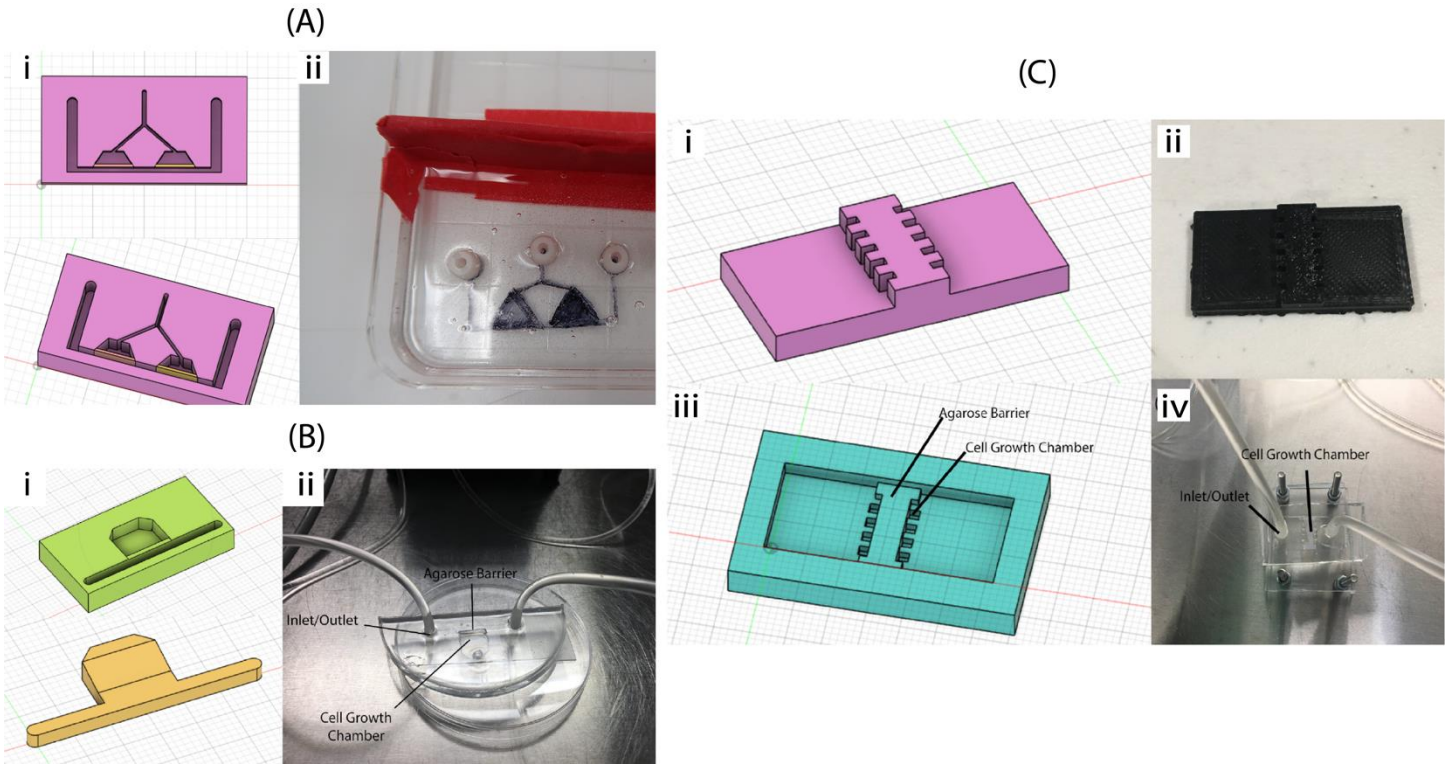

FIGURE 2. (A) First design with two cell growth chambers (i) CAD design with orange and yellow blocks signifying the agarose barrier (ii) first prototype mold in PDMS during solidifying process. (B) Second design with horizontal axis and one cell growth chamber (i) CAD model of PDMS cast from design (ii) CAD model of 3D printed mold design (iii) Prototype of second design on a glass slide fitted with input and output tubes. (C) Final prototype design (i) CAD design of mold (ii) CAD model of PDMS cast (iii) 3D-printed mold for prototype (iv) Final tumor-on-chip device.

The second device schematic utilized a horizontal layout that combined the two cell growth chambers to increase the surface area for the cells to spread. This model used a 3D-printed mold and glass slide base. This change made the cells more visible and resulted in clear images of the entire device. Cells grown in this model were once again separated from the medium channel by a 1% agarose barrier. It was clear that there was a consistent cell monolayer that was produced in the farthest three-fourths of the cell growth chamber from the medium channel. In the area closest to the medium channel, the fluid dynamics resulted in higher pressure closer to the barrier. This pressure resulted in more cell clusters being formed at the agarose barrier. These cells quickly died from the pressure within a day, and there were small amounts of cell clusters, with an average of 2 for ten trials conducted using this prototype.

The final prototype used both the horizontal and vertical axis to exact shear force on the cells and promoted three-dimensional tumoroid structure formation. The device was created using a 3D-printed mold with eight cell-growth chambers, each separated by an agarose barrier.

Above the chambers ran a medium channel that allowed for waste removal and nutrient exchange and exacted force on the cells, which did not allow a typical monolayer to form. This prototype produced an average of eight tumoroids per device throughout ten trials, with a near 100% success rate for each tumor growth chamber. The tumoroids produced survived for two to three days and displayed characteristics such as motility into the agarose barrier and a

clear three-dimensional structure. The final prototype improved on past prototypes with a plexiglass base and ceiling, ensuring that the device could be sterile and the PDMS was untouched.

Analyzing Heterogeneity

After a successful device was created that could model the cancer environment and create tumoroids consistently, the tumoroids' heterogeneity was analyzed through microscopy and a cell counter. As a control, a flask of A549 cells was grown alongside the device. These cells produced a consistent monolayer in the flask, and when measured using a cell counter, had an average cell size of 17.72 micrometers. The cells had the distinct rhombus cell shape of A549 cells that were grown in a monolayer. They featured little cell motility when imaged every four hours using a light microscope. After growth in the flask at a 0.5 x 10^6 cells/mL dilution, the final cell density of this culture was 4.96 $10^{0.5}$ cells/mL. Exact cell density varied throughout imaging, with no more than one cell occupying a space.

Ten trials were conducted using the final prototype that contained eight tumoroid growth chambers. Three common subtypes were identified based on quantitative factors (Figure 3). The first subtype was small-diameter, high motility cells which averaged 13.37 micrometers with a standard deviation of 2 micrometers in cell diameter. These A549 cells demonstrated consistent cell cycle patterns as they were mainly in the second growth and mitotic phase. The cell cycle pattern was visualized using the cell cycle fluorescence marker, FUCCI Cell Cycle Sensor, which displays green fluorescence when staining cells in G2 and mitotic stages. The tumor cell subtype migrated at an average pace of 0.5 cm/hr with a standard deviation of 0.02 cm/hr. Tumors with these cells also invaded into the agarose barrier, demonstrating metastasis characteristics and aggressiveness.

The second subtype that was viewed at a lower frequency was medium-diameter, low motility cells dormant within the tumoroid. These cells showed necrosis or dormancy characteristics, with live cells displaying red fluorescence from the FUCCI marker, demonstrating that they were in the first growth phase or dormant. The subtype did not migrate and averaged a cell diameter of 16.72 micrometers with a standard deviation of 0.8 micrometers.

The final cell subtype characterized was medium diameter, mid-motility cells identified primarily on the outer edges and middle layers of tumoroid analyzed. These cells had an average cell diameter of 17.54 micrometers with a standard deviation of 1.2 micrometers. They had a more extensive range of motility with an average migration rate of 0.2cm/hr and a standard deviation of 0.07 cm/hr. This cell subtype also

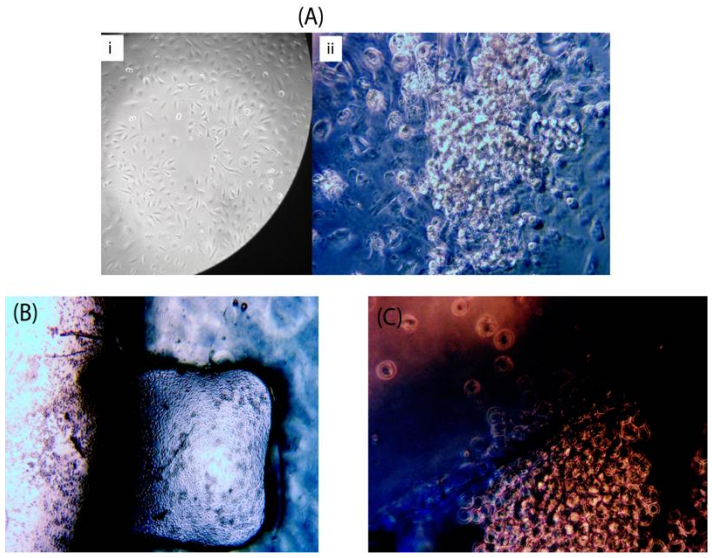

FIGURE 3. (A) Comparison of tumoroid in tumor-on-chip device to cell monolayer imaged using light microscope (i) monolayer of cells in flask with rhombus shape (ii) Tumoroid in tumor-on-chip device. (B) Example of aggressive tumoroid invading into the agarose barrier. (C) Cells in cancer growth chamber in tumor-on-chip device.

stained green from the FUCCI marker, demonstrating that they were either in the second growth phase or mitosis. These cells were the most common subtype of cells found in the tumoroids. Many of these cells also formed small clusters surrounding the tumoroids. Smaller proportions of cells displaying other combinations of these characteristics were also visualized.

The control of the cells in the flask had a large difference in cell characteristics. The control A549 cells differed in cell shape, with most cells in the control flask sharing a rhombus shape compared to the circular cells found in the device. The control cells had a smaller range in cell size than the device's cells, with a consistent cell size of 17.72um and average standard deviation of 0.4 micrometers, no cell motility, and no cell cycle patterns spatially.

The differences in cell size were checked based on a 99.5% t-test to compare the significance of the differences. For both the quantitative factors of cell size and cell motility, each subtype's average was to the control as well as to the other subtypes to determine significance.

Apart from these three subtypes, the device created tumoroids that displayed intertumoral heterogeneity in two primary factors varied: motility and extracellular matrix production. Of the 82 tumoroids imaged, 28 of these tumoroids produced an extracellular matrix visible through the microscope. A higher proportion of these tumoroids had high motility, with 65 of the 82 tumoroids imaged invading into the agarose barrier at the end of the experiment.

Discussion

Through prototyping and a series of experiments, a tumor-on-a-chip device was created that allowed for the isolation and study of independently forming three-dimensional tumoroids in an environment that mimics the human body. Different variables were tested during the optimization process that contribute to more accurate tumor-on-chip devices. Both petri dishes and glass slides were tested as bases for cells to attach. These alternatives had limitations because they could not seal the PDMS, limiting tests to one use per device. The final prototype used two plexiglass sheets that were drilled at points to create inlets and outlets for tubes transporting medium and holes to clamp the two sheets together, sealing the PDMS. Determining the cancer chamber's size and placement to allow shear force to induce three-dimensional tumor formation also posed a challenge. With earlier prototypes, the chamber was placed on a horizontal plane next to the channel transporting medium, which allowed cells to form a monolayer. The device's final design proved that the chamber's optimal placement was below the channel, where pressure from the medium flowing above the cells forced them to group together.

This device produced tumoroids without the aid of a scaffold or hanging drop, as found in other methods. Instead, the device allowed for the natural creation of tumoroids, providing a more accurate model of cell-cell interactions and the biophysics that allow for tumoroid production. The model created allows for the analysis of multiple phenotypic factors in the tumoroids through microscopy and fluorescence imaging, providing a lens to better capture the tumor's progression (Table 1; Figure 4). The device also creates an environment that mimics the human body's blood vessels, with medium flowing through a channel and nutrient diffusion occurring between the cells and the "blood vessel".

As shown by quantitative data, intra-tumoral heterogeneity could also be analyzed with multiple cell subtypes identified, including the three common subtypes: small diameter and high motility on the fringe of the tumoroid, mid-diameter and dormancy in clusters around the tumoroid, and mid-diameter and mid-motility found throughout the masses created. These different cell subtypes demonstrate the efficacy of the device, which were paired together to analyze intratumoral factors and identify aggressive tumoroids. The behaviors of cell densities, cell diameters, and cell motility demonstrate that intratumoral heterogeneity can be analyzed using this microfluidic model.

TABLE 1. Chart of intratumoral factors measured and common cell subtypes identified in tumoroids imaged (n=82).

	Cell Intratumoral Heterogeneity Factors						
	Freq (%)	Cell Size (um) Average	Cell Size (um) Standard Deviation	Cell Motility (cm/hr) Average	Cell Motility (cm/hr) Standard Deviation	Cell Cycle Pattern	Location in Tumoroid
Control (Cells in Flask)	N/A	17.72	0.4	0	0	Mixed	Monolayer
Cell Subtype 1	11%	13.37	2	0.5	0.2	Growth 2/Mitosis	Outer Edges of Tumor
Cell Subtype 2	32%	16.72	0.8	0	0	Growth 1	Center/Clusters in Tumor
Cell Subtype 3	48%	17.54	1.2	0.2	0.07	Growth 2/Mitosis	Throughout Tumor

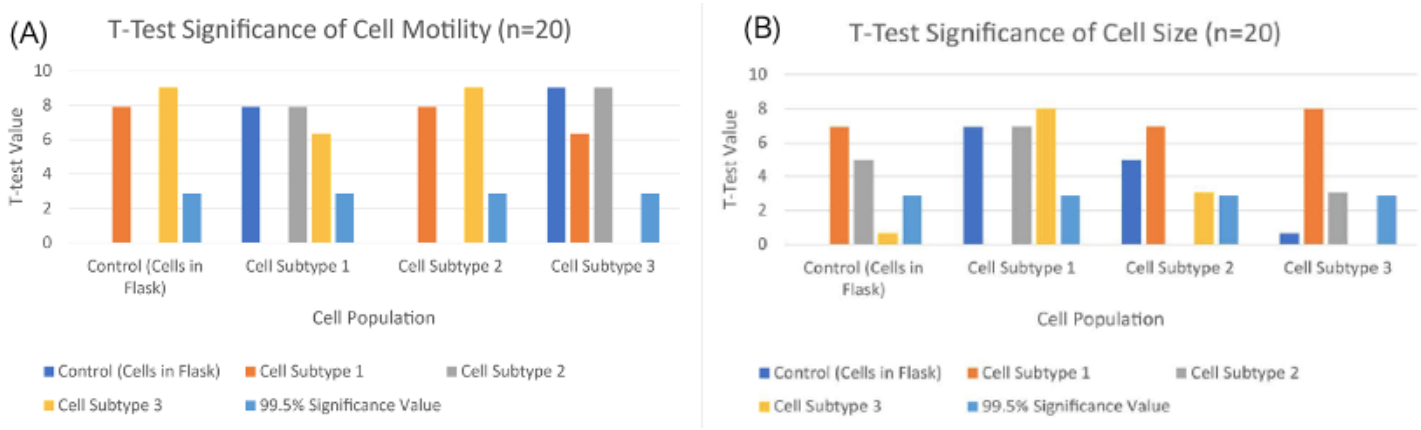

FIGURE 4. (A) Significance Comparison of Cell Motility using 99.5% T-Test. (B) Significance Comparison of Cell Size using 99.5% T-Test.

To improve this model, more phenotypic characteristics of tumors should be analyzed to test the device's limitations. The device may be more optimized by testing more variables such as medium flow, to accurately simulate the human body's environment. The device may also incorporate different cell lines such as human umbilical vein endothelial cells (HUVECs) and immune cells to create an environment that better represents the heterogeneity and cancer-immune cell interaction that occurs in the tumor microenvironment. Experiments regulating the CO2 and O2 concentrations would also create an environment more akin to the human body with biochemical gradient simulation. With a confocal incubator microscope, a z-stack could be created of the tumoroids, and the study could occur in real-time to display the continuous interactions that occur in the device.

Cell monolayers, which are the industry standard for studying cancer, are not accurate for testing the effectiveness of cancer therapeutics and quantifying tumor resistance. This microfluidic device allows cells to form realistic three-dimensional tumoroids with biochemical and biophysical factors that enable cells to display intratumoral heterogeneity. In addition, drugs can be incorporated into the medium channel to test their efficacy, producing a more regulated environment than three-

dimensional xenograft and animal models. With a more accurate drug testing model, cancer therapeutics can be tested against patient-derived cells in this microfluidic device to create a patient-specific personalized therapy based on the cell subtypes identified. Looking to the future, this microfluidic device can be used to test drugs, categorize tumor aggressiveness, and create more effective personalized therapy for patients.

References

Aaron S. M., Laura M. H. Systems biology approaches to measure and model phenotypic heterogeneity in cancer, Current Opinion in Systems Biology, Volume 17, 2019, Pages 35-40, ISSN 2452-3100, https://doi.org/10.1016/j.coisb.2019.09.002.

Ahmed, F., & Haass, N. K. (2018). Microenvironment-Driven Dynamic Heterogeneity and Phenotypic Plasticity as a Mechanism of Melanoma Therapy Resistance. *Frontiers in oncology*, *8*, 173. https://doi.org/10.3389/fonc.2018.00173

Balkwill, F. R., Capasso, M., & Hagemann, T. (2012). The tumor microenvironment at a glance. *Journal of cell science*, *125*(Pt 23), 5591–5596. https://doi.org/10.1242/jcs.116392

Ballotti, R., Cheli, Y., & Bertolotto, C. (2020). The complex relationship between MITF and the immune system: a Melanoma ImmunoTherapy (response) Factor?. *Molecular cancer*, *19*(1), 170. https://doi.org/10.1186/s12943-020-01290-7

Becher, O. J., & Holland, E. C. (2006). Genetically engineered models have advantages over xenografts for preclinical studies. *Cancer research*, *66*(7), 3355–3359. https://doi.org/10.1158/0008-5472.CAN-05-3827

Begley, C., Ellis, L. Raise standards for preclinical cancer research. *Nature* **483,** 531–533 (2012). https://doi.org/10.1038/483531a.

Bray, F., Ferlay, J., Soerjomataram, I., Siegel, R. L., Torre, L. A., & Jemal, A. (2018). Global cancer statistics 2018: GLOBOCAN estimates of incidence and mortality worldwide for 36 cancers in 185 countries. *CA: a cancer journal for clinicians*, *68*(6), 394–424. https://doi.org/10.3322/caac.21492

Cancer. *World Health Organization*. https://www.who.int/news-room/fact-sheets/detail/cancer.

Chapman, A., Fernandez del Ama, L., Ferguson, J., Kamarashev, J., Wellbrock, C., & Hurlstone, A. (2014). Heterogeneous tumor subpopulations cooperate to drive invasion. *Cell reports*, *8*(3), 688–695. https://doi.org/10.1016/j.celrep.2014.06.045

Gerlinger, M., Rowan, A. J., Horswell, S., Math, M., Larkin, J., Endesfelder, D., Gronroos, E., Martinez, P., Matthews, N., Stewart, A., Tarpey, P., Varela, I., Phillimore, B., Begum, S., McDonald, N. Q., Butler, A., Jones, D., Raine, K., Latimer, C., Santos, C. R., … Swanton, C. (2012). Intratumor heterogeneity and branched evolution revealed by multiregion sequencing. *The New England journal of medicine*, *366*(10), 883–892. https://doi.org/10.1056/NEJMoa1113205

Hanahan, D., & Weinberg, R. A. (2011). Hallmarks of cancer: the next generation. *Cell*, *144*(5), 646–674. https://doi.org/10.1016/j.cell.2011.02.013

Hutchinson, L., Kirk, R. High drug attrition rates—where are we going wrong?. *Nat Rev Clin Oncol* 8**,** 189–190 (2011). https://doi.org/10.1038/nrclinonc.2011.34

Mierke C. T. (2019). The matrix environmental and cell mechanical properties regulate cell migration and contribute to the invasive phenotype of cancer cells. *Reports on progress in physics. Physical Society (Great Britain)*, *82*(6), 064602. https://doi.org/10.1088/1361-6633/ab1628

Mierke C. T. (2014). The fundamental role of mechanical properties in the progression of cancer disease and inflammation. *Reports on progress in physics. Physical Society (Great Britain)*, *77*(7), 076602. https://doi.org/10.1088/0034-4885/77/7/076602

Oudin, M. J., & Weaver, V. M. (2016). Physical and Chemical Gradients in the Tumor Microenvironment Regulate Tumor Cell Invasion, Migration, and Metastasis. *Cold Spring Harbor symposia on quantitative biology*, *81*, 189–205. https://doi.org/10.1101/sqb.2016.81.030817

Ramón y Cajal, S., Sesé, M., Capdevila, C. *et al.* Clinical implications of intratumor heterogeneity: challenges and opportunities. *J Mol Med* **98,** 161–177 (2020). https://doi.org/10.1007/s00109-020-01874-2

Redmon, J., Divvala, S., Girshick, R. B., Farhadi, A. (2015). You Only Look Once: Unified, Real-Time Object Detection. *CoRR*. http://arxiv.org/abs/1506.02640

Riedl, A., Schlederer, M., Pudelko, K., Stadler, M., Walter, S., Unterleuthner, D., … Dolznig, H. Comparison of cancer cells in 2D vs 3D culture reveals differences in AKT–mTOR–S6K signaling and drug responses. Journal of Cell Science. https://jcs.biologists.org/content/130/1/203.

Rhim, J. S., Tsai, W. P., Chen, Z. Q., Chen, Z., Van Waes, C., Burger, A. M., & Lautenberger, J. A. (1998). A human vascular endothelial cell model to study angiogenesis and tumorigenesis. *Carcinogenesis*, *19*(4), 673–681. https://doi.org/10.1093/carcin/19.4.673

Werner, H. M., Mills, G. B., & Ram, P. T. (2014). Cancer Systems Biology: a peek into the future of patient care?. *Nature reviews. Clinical oncology*, *11*(3), 167–176. https://doi.org/10.1038/nrclinonc.2014.6

Yuan Y. (2016). Spatial Heterogeneity in the Tumor Microenvironment. *Cold Spring Harbor perspectives in medicine*, *6*(8), a026583. https://doi.org/10.1101/cshperspect.a026583